SUPPORTING INFORMATION

for

Differential Deformability of the DNA Minor Groove and Altered BI/BII Backbone Conformational Equilibrium by the Monovalent Ions Li^+, Na^+, K^+ and Rb^+ via Water-Mediated Hydrogen Bonding

Alexey Savelyev and Alexander D. MacKerell Jr.*

Department of Pharmaceutical Sciences, School of Pharmacy, University of Maryland, Baltimore, MD 21201

* Corresponding author

Mailing Address: 20 Penn Street, Room 629, Baltimore, MD 21201

Email: alex@outerbanks.umaryland.edu

Phone: (410) 706-7442

Fax: (410) 706-5017

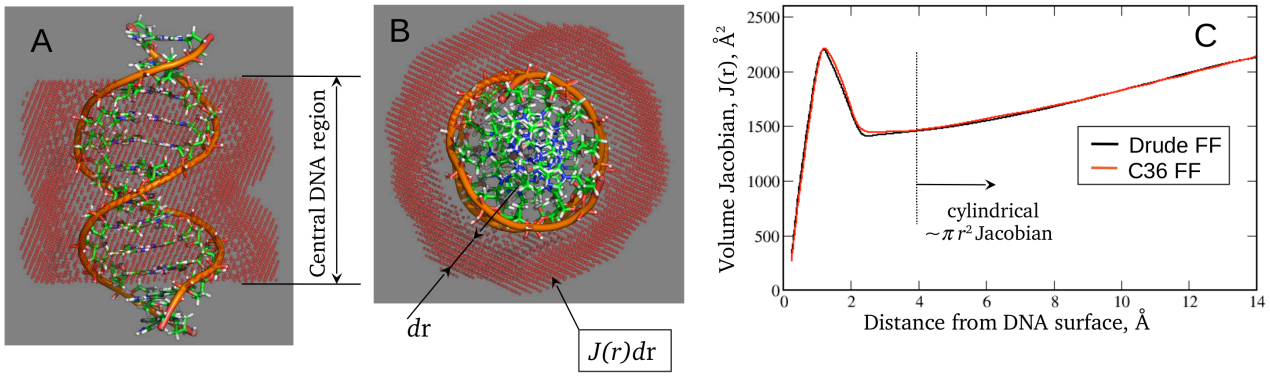

Figure S1. Side (A) and top (B) views of the DNA and equidistant shell (in red) from its surface. The shell's thickness is *dr* and its volume is *J(r)dr*. *J(r)* is the volume Jacobian whose numerical value as a function of the distance from DNA surface is shown in C. It is seen that only after ~4 Å from DNA, the function is monotonically increasing and can be approximated by the cylindrical Jacobian often used for calculation of the ionic distributions around DNA. To avoid end effects, ionic distributions were analyzed in the central region of the DNA, as shown in A.

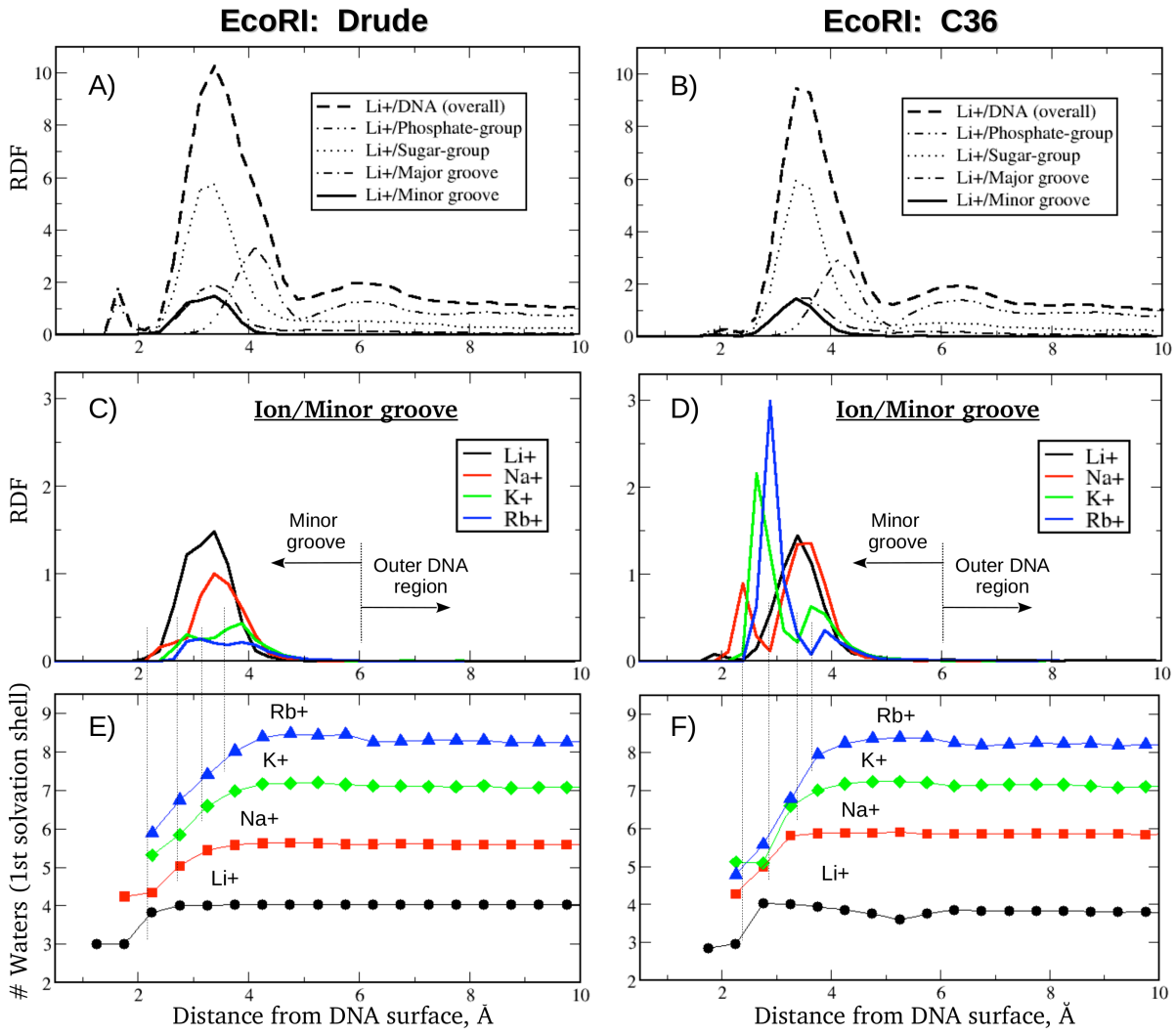

Figure S2. Analysis of the DNA minor groove occupancy by different monovalent ions and the ionic hydration patterns from MD simulations of the Drude polarizable (left) and C36 additive (right) EcoRI system. (A, B) An overall ion-DNA RDF is decomposed into contributions from ionic structuring around different DNA atomic selections; the case of Li^+ distributions is shown. (C, D) Ionic structuring of the Li^+, Na^+, K^+ and Rb^+ ions around the DNA minor groove. (E, F) Number of waters in the first solvation shells of the Li^+, Na^+, K^+ and Rb^+ ions as functions of the ion's distance from the DNA surface. Positions separating the first and second minima of the Ion/Minor-groove RDFs are projected (dotted lines) onto the ionic solvation curves.

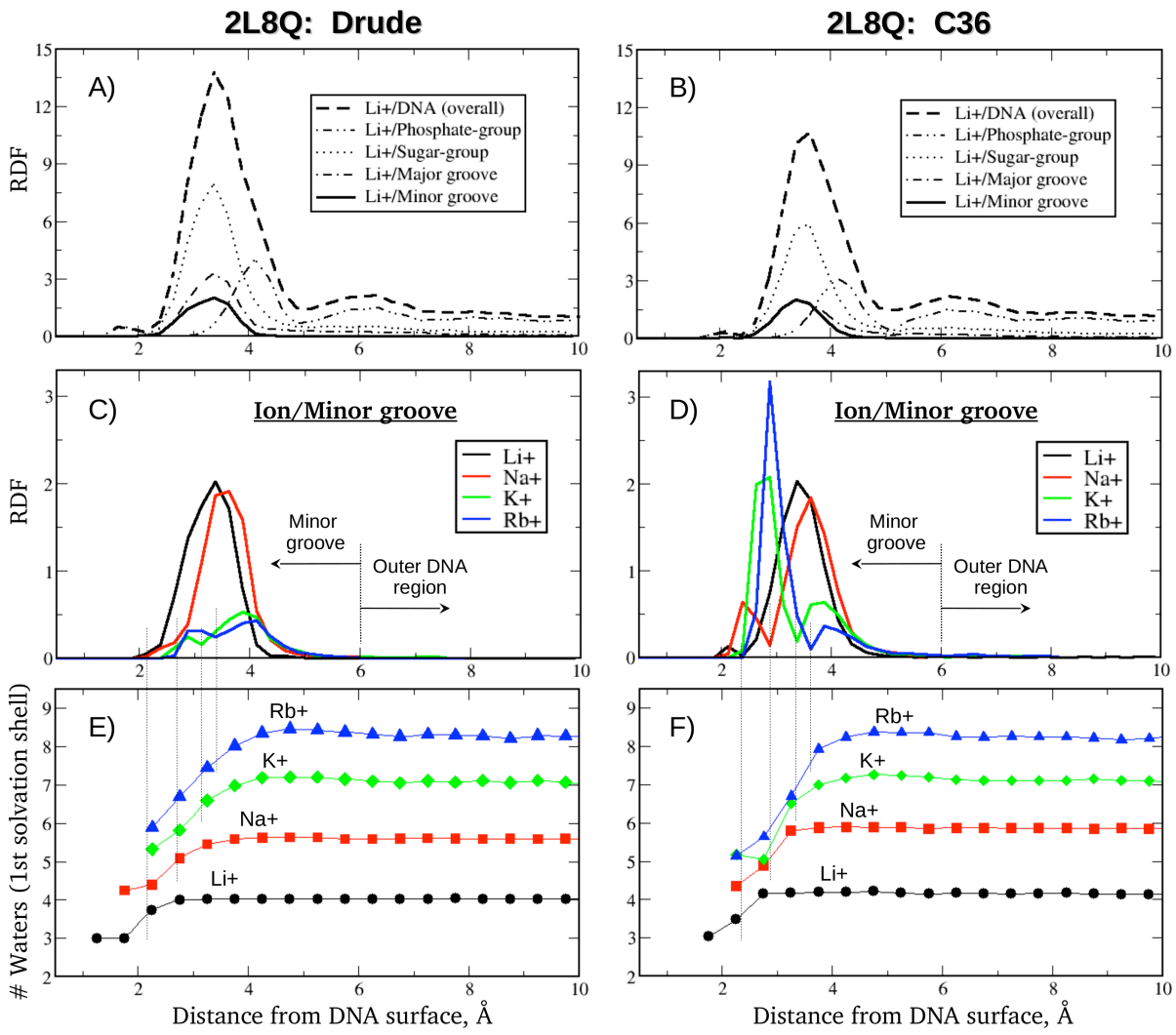

Figure S3. Analysis of the DNA minor groove occupancy by different monovalent ions and the ionic hydration patterns from MD simulations of the Drude polarizable (left) and C36 additive (right) 2L8Q system. (A, B) An overall ion-DNA RDF is decomposed into contributions from ionic structuring around different DNA atomic selections; the case of Li^+ distributions is shown. (C, D) Ionic structuring of the Li^+, Na^+, K^+ and Rb^+ ions around the DNA minor groove. (E, F) Number of waters in the first solvation shells of the Li^+, Na^+, K^+ and Rb^+ ions as functions of the ion's distance from the DNA surface. Positions separating the first and second minima of the Ion/Minor-groove RDFs are projected (dotted lines) onto the ionic solvation curves.

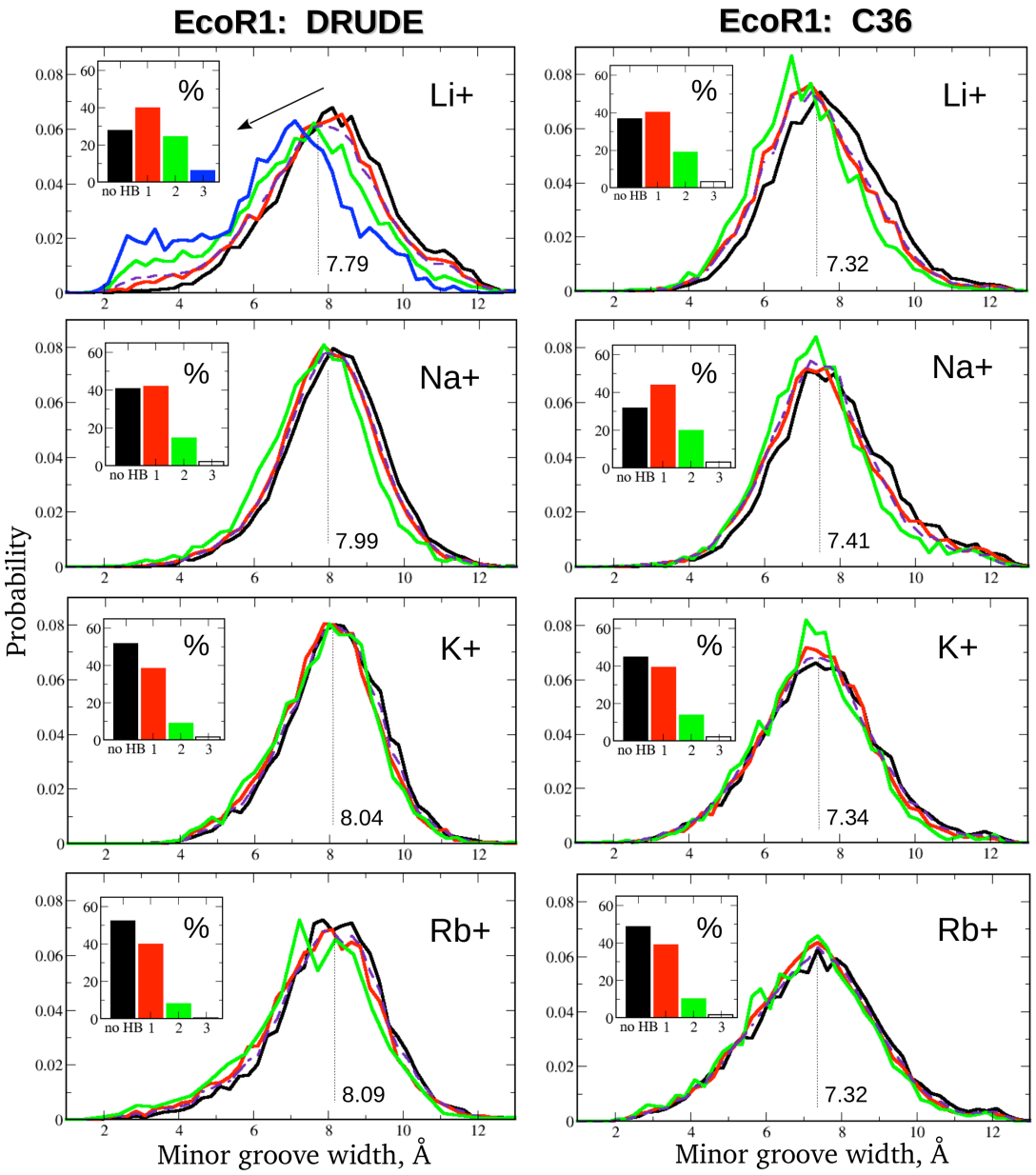

Figure S4. Relationship between the number of the SIS–HBB complexes formed along the EcoRI oligomer and the size of the minor groove. Results for the LiCl, NaCl, KCl and RbCl salt buffers with the Drude polarizable (left) and C36 additive (right) models are shown. Red and green curves denote minor groove width probability distributions corresponding to occurrence of one and two SIS–HBB complexes, respectively; black curves indicate the distributions in the absence of SIS–HBBs; dashed purple curves and the values represent the minor groove width distributions and the corresponding averages inferred from the entire MD trajectories. Insets show the time fractions of various binding events. Arrows are placed to emphasize the effect of the increase in the number of the SIS–HBB complexes formed on the minor groove size.

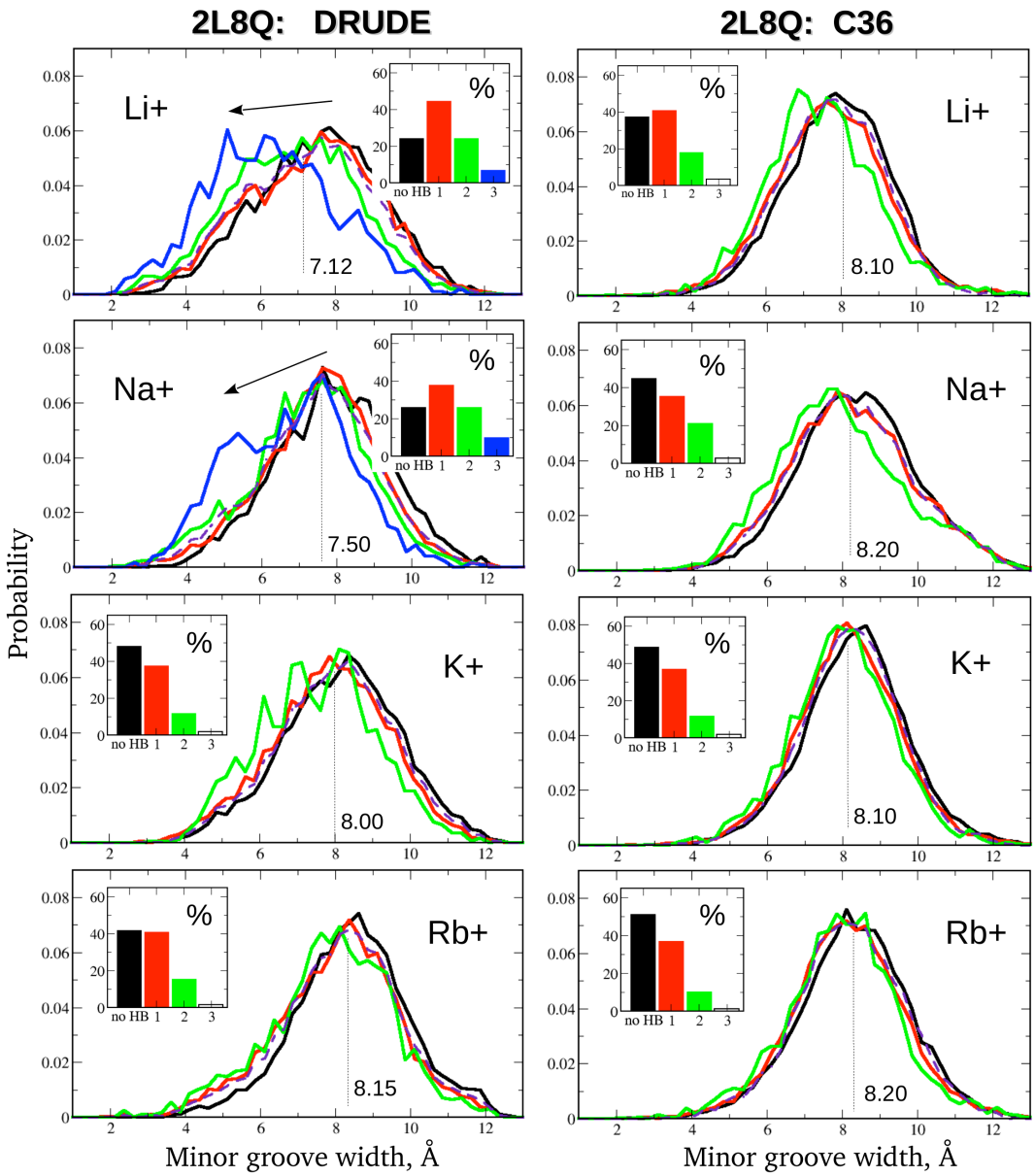

Figure S5. Relationship between the number of the SIS–HBB complexes formed along the 2L8Q oligomer and the size of the minor groove. Results for the LiCl, NaCl, KCl and RbCl salt buffers with the Drude polarizable (left) and C36 additive (right) models are shown. Red and green curves denote minor groove width probability distributions corresponding to occurrences of one and two SIS–HBB complexes, respectively; black curves indicate the distributions in the absence of SIS–HBBs; dashed purple curves and the values represent the minor groove width distributions and the corresponding averages inferred from the entire MD trajectories. Insets show the time fractions of various binding events. Arrows are placed to emphasize the effect of the increase in the number of the SIS–HBB complexes formed on the minor groove size.

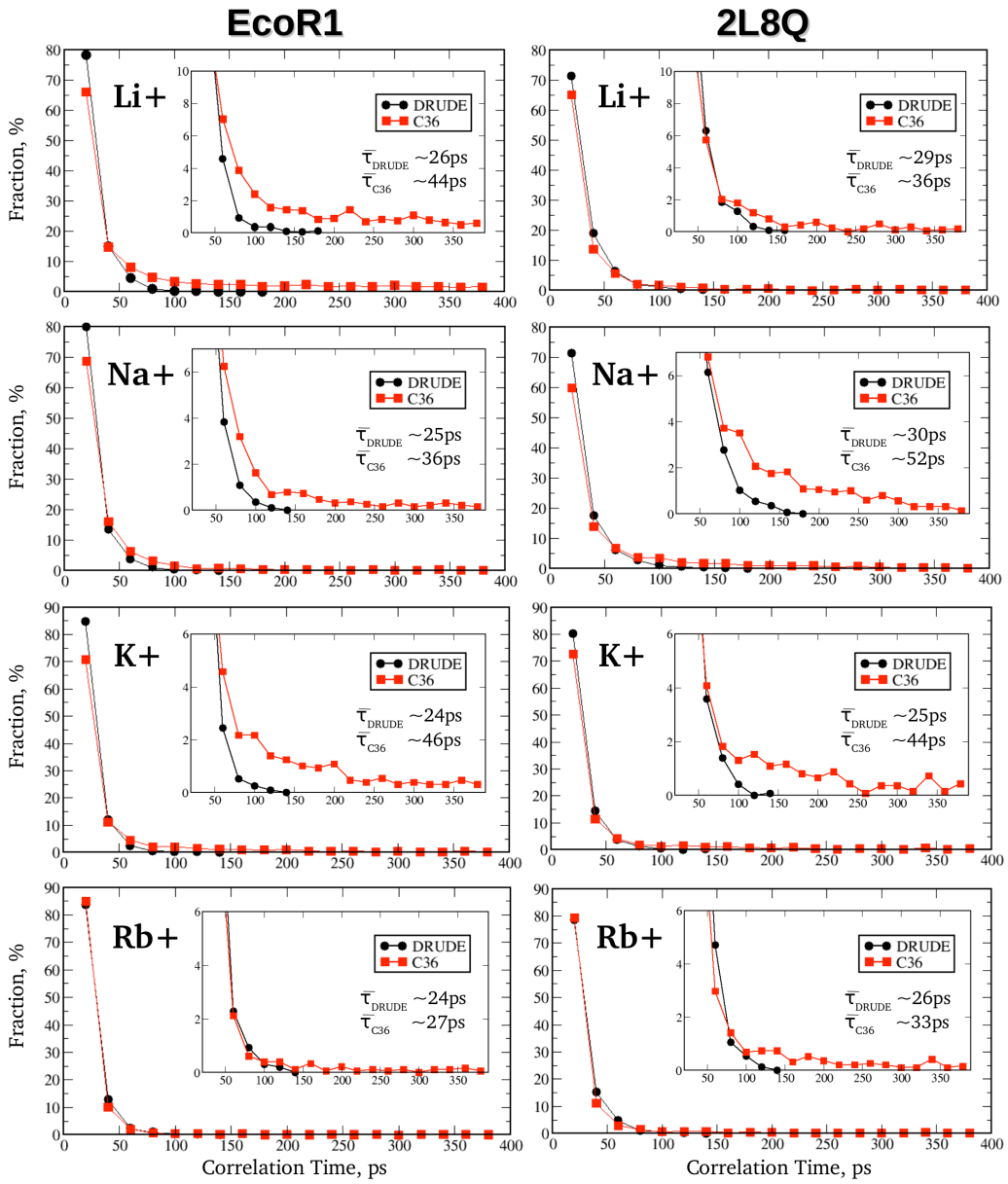

Figure S6. Lifetime probability distribution functions of the SIS–HBB complexes formed along EcoRI (left) and 2L8Q (right) oligomers involving different monovalent ions from the Drude polarizable (circles) and C36 additive (squares) MD simulations. Average lifetimes derived from these distributions are provided in the insets.

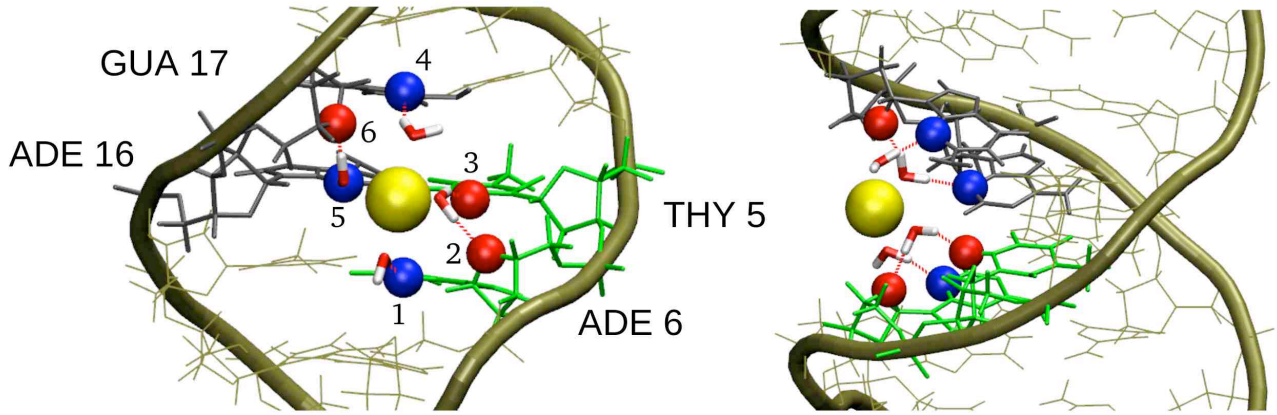

Figure S7. MD simulation snapshot (side and top views) illustrating that several water mediated hydrogen bonds contribute to maintaining a SIS–HBB complex. Shown is an example of the 1DCV duplex whose strands are mediated by solvated Na^+ ion (yellow). Hydrogen bonds 1, 2, 3 and 4, 5, 6 are formed with atoms N3:ADE6, O4':ADE6, O2:THY5 of strand 1 (green) and atoms N3:GUA17, N3:ADE16, O4':GUA17 of strand 2 (dark grey), respectively. The listed DNA atoms involved in the hydrogen bonds are shown as spheres for the oxygens (red) and the nitrogens (blue).

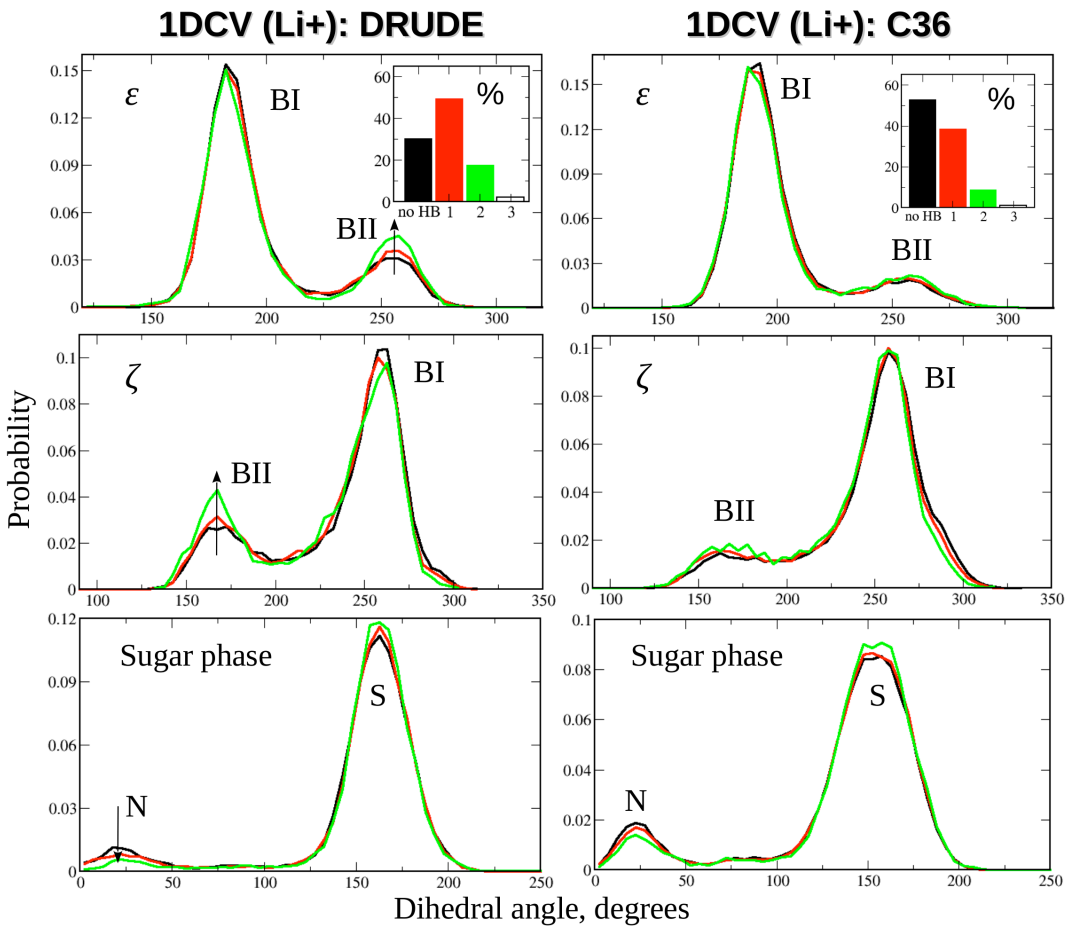

Figure S8. Influence of the number of the SIS–HBB complexes on the conformation of the DNA backbone and sugar moiety. Shown are the probability distribution functions for the ε and ζ dihedral angles of the backbone and pseudorotation angle of the sugar moiety from the Drude (left) and C36 (right) MD simulations of the 1DCV system in LiCl salt buffer. Coloring of the distributions and the time fractions in the insets is the same as in Fig. 3 of the main text. Arrows indicate the increase in the population of the BII substate of the backbone (ε, ζ) and decrease in the north (N) population of the sugar group as the number of SIS–HB complexes formed along DNA oligomer increases from zero (black) to one (red) to two (green).

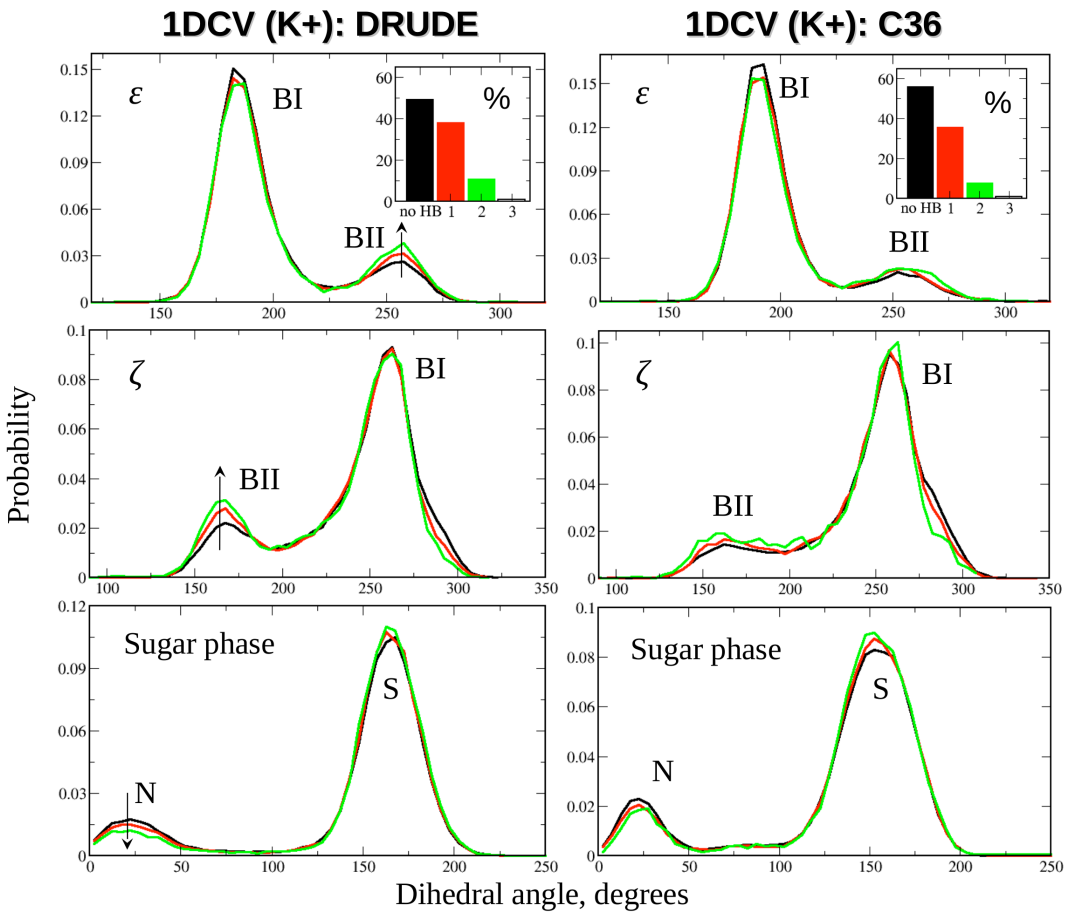

Figure S9. Influence of the number of the SIS–HBB complexes on the conformation of the DNA backbone and sugar moiety. Shown are the probability distribution functions for the ε and ζ dihedral angles of the backbone and pseudorotation angle of the sugar moiety from the Drude (left) and C36 (right) MD simulations of the 1DCV system in KCl salt buffer. Coloring of the distributions and the time fractions in the insets is the same as in Fig. 3 of the main text. Arrows indicate the increase in the population of the BII substate of the backbone (ε, ζ) and decrease in the north (N) population of the sugar group as the number of SIS–HB complexes formed along DNA oligomer increases from zero (black) to one (red) to two (green).

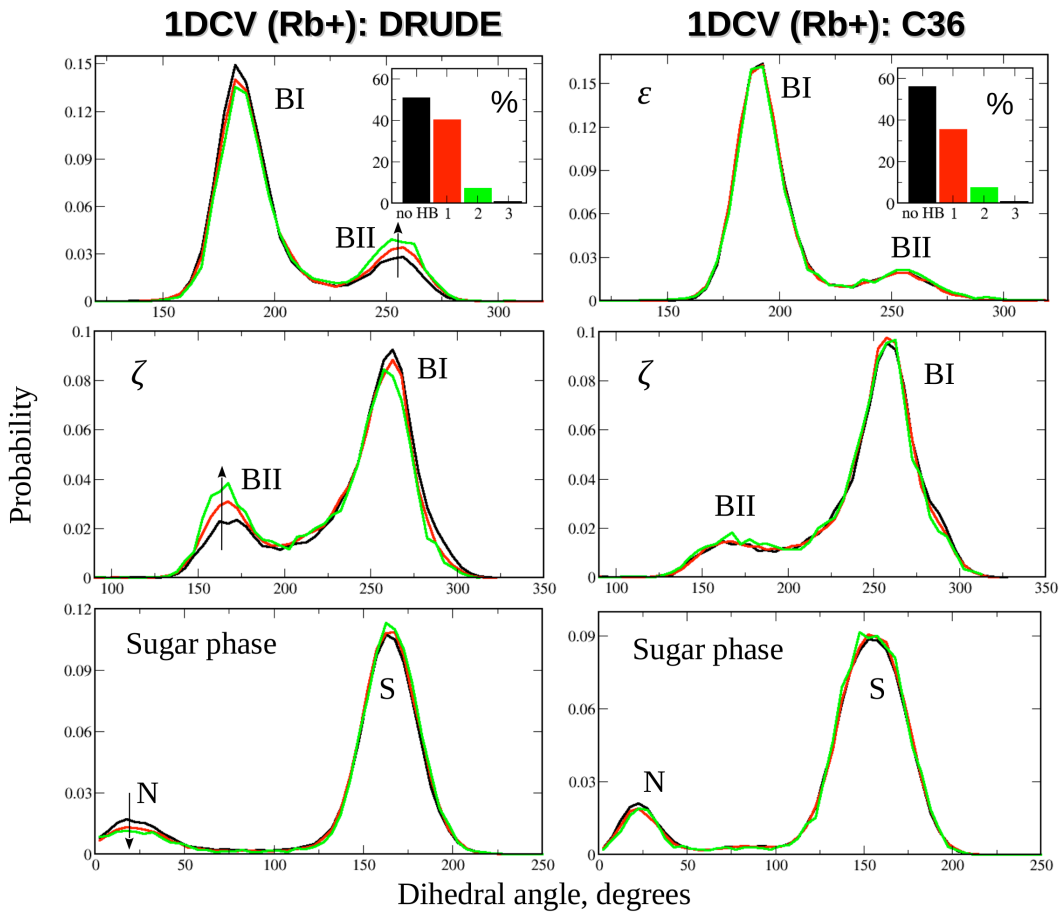

Figure S10. Influence of the number of the SIS–HBB complexes on the conformation of the DNA backbone and sugar moiety. Shown are the probability distribution functions for the ε and ζ dihedral angles of the backbone and pseudorotation angle of the sugar moiety from the Drude (left) and C36 (right) MD simulations of the 1DCV system in RbCl salt buffer. Coloring of the distributions and the time fractions in the insets is the same as in Fig. 3 of the main text. Arrows indicate the increase in the population of the BII substate of the backbone (ε, ζ) and decrease in the north (N) population of the sugar group as the number of SIS–HB complexes formed along DNA oligomer increases from zero (black) to one (red) to two (green).